EPJ Web of Conferences **6**, 20003 (2010)
DOI:10.1051/epjconf/20100620003

Real time sensing of structural glass fiber reinforced composites by using embedded PVA - carbon nanotube fibers

Nikolaos D. Alexopoulos[1,2a], , Phillipe Poulin[3] , Christele Bartholome[3], and Zaira Marioli-Riga[1]

[1]Hellenic Aerospace Industry, Research and Development Department, 320 09 Schimatari, Greece
[2]University of the Aegean, Department of Financial Engineering, 821 00 Chios, Greece
[3]Université de Bordeaux, Centre de Recherche Paul Pascal – CNRS, Avenue Schweitzer, 33600 Pesseac, France

Abstract. Polyvinyl alcohol - carbon nanotube (PVA-CNT) fibers had been embedded to glass fiber reinforced polymers (GFRP) for the structural health monitoring of the composite material. The addition of the conductive PVA-CNT fiber to the non-conductive GFRP material aimed to enhance its sensing ability by means of the electrical resistance measurement method. The test specimen's response to mechanical load and the in situ PVA-CNT fiber's electrical resistance measurements were correlated for sensing and damage monitoring purposes. The embedded PVA-CNT fiber worked as a sensor in GFRP coupons in tensile loadings. Sensing ability of the PVA-CNT fibers was also demonstrated on an integral composite structure. PVA-CNT fiber near the fracture area of the structure recorded very high values when essential damage occurred to the structure. A finite element model of the same structure was developed to predict axial strains at locations of the integral composite structure where the fibers were embedded. The predicted FEA strains were correlated with the experimental measurements from the PVA-CNT fibers. Calculated and experimental values were in good agreement, thus enabling PVA-CNT fibers to be used as strain sensors.

1 Introduction

Glass fiber reinforced polymers (GFRP) are widely used in the aeronautical and the automotive industry mainly due to their high specific mechanical properties. During the last decades, the aerospace industry focus its research in producing multi-functional materials, driving design parameters being the weight reduction with increased mechanical properties as well as monitoring their structural health by means of sensing capability.

The electric resistance change method had been firstly used by Schulte and Baron [1] for sensing of the structural health monitoring, by means of identifying internal damage of carbon fiber reinforced (CFRP) laminates. The electrical conductivity of the carbon fibers was used to monitor damage in carbon fibre reinforced polymers (CFRPs), and for a variety of damage mechanisms, e.g. delamination, matrix cracking, under various loading conditions, e.g. [2].

[a] Corresponding author, e-mail: nalexop@tee.gr

Exploiting the electrical conductivity of the carbon nanotubes (CNT), they could be used to non-conductive composite materials in order to enhance their monitoring capabilities. The addition of CNT's to the polymer matrix of non-conductive composite materials such as the GFRP material (also called as doped resin), made the epoxy matrix electrically conductive. This enables to fully monitor the structural health of GFRPs with doped resin and establish correlations between internal damage and increase in resistance, e.g. [3, 4].

Notice that the monitoring of carbon fibre composites is also feasible; they have inherent conductivity and their sensing ability has been performed in the literature during the last two decades, e.g. [3, 5]. The idea of monitoring a composite using a unique conductive fiber has been made in [6], where a carbon fiber was embedded into GFRP coupons. Using the electrical conductivity of an embedded fiber into non-conductive composites, the structural health monitoring can be assessed by the in-situ measurements of the inherent electrical resistance change of the fiber. However, mainly due to the difference in modulus of elasticity between the two medias in the above referred case, the sensor 'carbon fiber' didn't actually monitor the progressive damage of the composite but more or less prognosed its final fracture.

Polyvinyl alcohol-carbon nanotube (PVA-CNT) fibers can be spun by injection of carbon nanotubes suspension through an orifice into a co-flowing stream of a coagulating solution [7, 8]. This can be achieved by mixing the CNT dispersion into an aqueous solution that contains a polymer (e.g. PVA) as coagulating agent. The PVA-CNT fibers have actually the size of a human hair and offer a promise for high strength, light weight, thermally and electrically conducting structural elements at a lower cost than other nanotube forms.

In the present work, polyvinyl alcohol carbon nanotube (PVA-CNT) fibers will be embedded to glass fiber reinforced composites and will be used for real-time sensing of such materials. Sensing ability of the hybrid composites will be demonstrated; this will be performed via coupon testing as well as via integral composite structure testing.

2 Material Manufacturing and Experimental Procedure

The materials used for the manufacture of the flat composite material plates with embedded carbon nanotube fibers were (a) multi-wall carbon nanotube (CNT) fibers prepared using a coagulation process, (b) epoxy resin Araldite LY564 / hardener Aradur 2954 supplied by Hunstman Advanced Materials, Bergkamen, Germany (ratio 100:35 parts by weight) and (c) glass fiber fabric PW, Style 6781 (S2-glass) by Fiber Glast Developments Corporation.

The PVA-CNT fiber manufacturing process consisted in injecting an aqueous carbon nanotube dispersion into the co-flowing stream of a coagulating polyvinyl alcohol solution. The nanotube dispersion is stabilized by sodium dodecyl, an anionic surfactant. The PVA polymer was purchased from Seppic – France. It has a molecular weight of 195000 g/mol and a hydrolysis ratio of 99%. More details regarding the manufacturing process of the fiber can be seen in [7-9].

2.1 Coupons manufacturing

The manufacturing of the hybrid composite material was made at Hellenic Aerospace Industry (HAI) and was extensively described elsewhere [10]. Briefly, 10 plies of fabric, oriented at 0/90° had been cut at the required dimensions (300 x 300 mm). The first 9 plies were laid and the wrap faces were alternated upwards and downwards during the lay-up, resulting in a cross-ply balanced and symmetric laminate. The PVA-CNT fibers were placed between the 9th and last ply of the composite. In total six PVA-CNT fibers were used per manufactured composite plate; this permitted the manufacturing of six testing specimens with one embedded fiber per specimen.

The specimens with the PVA-CNT fiber had been cut from the material plates according to the ASTM D3039 specification and edge-polished (Figure 1). The dimensions of the testing specimens were width x length = 25 mm x 250 mm. At the two marks of each specimen covered with silver

paste, two cable connectors had been added again with silver paste in order to attach the multimeter for the resistance measurements.

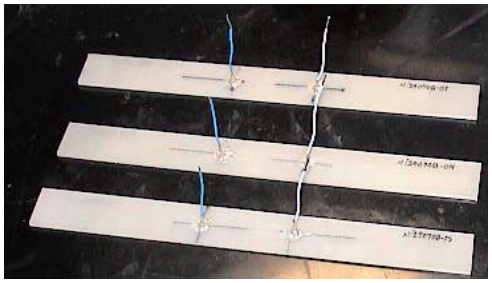

Fig. 1. Photograph of manufactured test specimens with embedded PVA-CNT fiber.

2.2 Integral structure manufacturing

For the manufacturing of the structure with the double T stiffeners that will be monitored using CNT fibers, the following process was followed: First the dry fabric was cut in the required dimensions (plate and stiffeners), and the vacuum infusion method had been employed at Hellenic Aerospace Industry (HAI). Four plies of fabric were laid for the skin, oriented at [0/45]s (Figure 2a). The lay-up for the T stiffeners can also be seen in the respective Figure.

The first 3 plies were first laid and the PVA-CNT fibers were placed (between the 3rd and last ply). Five PVA-CNT fibers were placed in such a way as can be seen in Figure 2a and with gauge length equal to 25 mm. Figure 2b shows a macro-photograph of the integral structure with electrical wiring system ready to be mechanically tested.

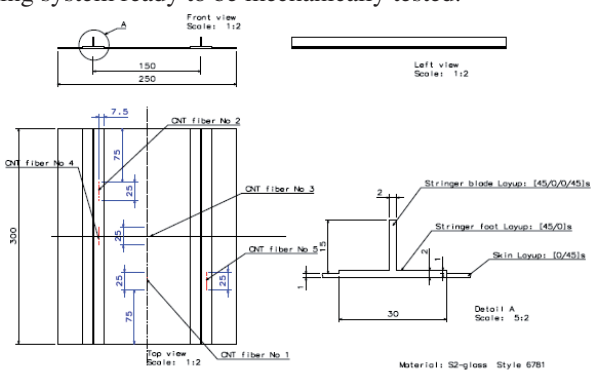

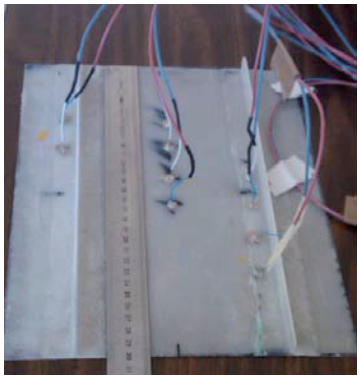

(a) (b)

Fig. 2. (a) Sketch and (b) photograph of the integral structure with the embedded PVA-CNT fibers.

2.3 Experimental procedure

Two different mechanical tests were conducted and the potential for electrical conductivity measurements for structural health monitoring was evaluated: (a) progressive damage accumulation (PDA) tests on coupons (incremental loading – unloading steps) and (b) the three-point bending test on the integral structure. A servo-hydraulic Instron 100 kN testing machine had been used to record the force and displacement data, while a 50 mm extensometer was attached to record axial strain data of the coupons.

An Agilent multimeter was used to record in situ the electrical resistance data of the specimen's embedded PVA-CNT fiber during mechanical loading. A DC voltage of 10 V was applied to cables connected to the PVA-CNT fiber of the specimens, the current was measured and the resistance was calculated from these values. The resistance measurements were performed in a two-point measurement set-up in the longitudinal direction. Data acquisition of 1 Hz was used for the

resistance measurements and stored simultaneously in the P/C of the testing machine. A rubber mat was placed between the specimen and the metal grip of the test machine in order to insulate the specimen from the test machine. Same procedure had been followed for the testing of the composite structure, while force, displacement and electrical measurements from all embedded PVA-CNT fibers were simultaneously recorded.

3 Results

3.1 Coupon tensile test

Test results for the tensile progressive damage accumulation tests in coupons can be graphically seen in Figure 3. Seven incremental loading – unloading steps had been performed; they corresponded to a specific percentage of the fracture stress (tensile strength R_m) of the coupon, respectively. In the Figure, the mechanical stress variation as well as the CNT fiber's electrical resistance $\Delta R/R_0$ variation can be seen. After the first three loading – unloading steps, the electrical resistance of the material remained the same (655 kΩ). An electrical resistance hysteresis was formed in the third loading; the loading and unloading branch can be clearly seen. After the unloading of the third step, a residual resistance was measured (658 kΩ), which can be interpreted as possible damage in the material or in the fiber. All loadings at higher stress level showed similar electrical behaviour; an electrical resistance hysteresis was noticed as well as incremental residual resistance after every unloading step.

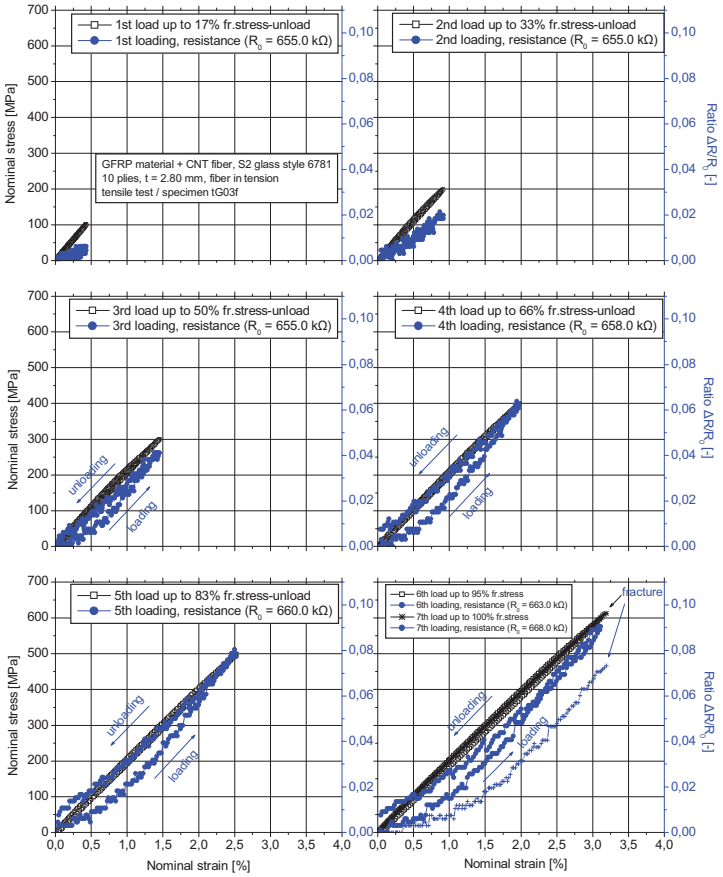

Fig. 3. Typical tensile mechanical and electrical resistance results of a GFRP specimen with embedded PVA-CNT fiber for different incremental loading – unloading steps.

The residual electrical resistance of the PVA-CNT fiber after every incremental loading – unloading step might be attributed to the nature of the manufactured fiber. As the elastic regime limit of the PVA-CNT fiber corresponds to strain of the order of magnitude of 1 to 1.25%, it is eminent that there exists no accumulating damage during the loading – unloading step of the fiber below these threshold values. Hence, any observed residual resistance when the composite is loaded below these values can be directly attributed to damage of the composite material. It is not clear whether the residual resistance of the fiber for higher loadings is attributed to damage in the composite material or in the fiber.

A direct correlation between the mechanical stress and the $\Delta R/R_0$ measurements can be seen in Figure 4. Note that the nominal strain instead of the nominal stress could also be used for such a correlation, since they are linear connected via the modulus of elasticity *E*. Mechanical stress had been preferred since it is the material property that is widely used in the aeronautical design office. All seven loadings could be fitted by means of a parabolic or exponential growth expression. At the third loading, no essential shift of the exponential growth curve was noticed. For the following loading curves, the exponential curves begin to shift at the stress level of 220 to 250 MPa and of the value of 2% for the $\Delta R/R_0$ measurements. For any incremental loading step, the correlated curve is more shifted by means of an unknown to the authors' growth law. The stress level of 220 MPa is too high for the case of aeronautical materials; note that the fuselage and the skin materials are designed for tensile stresses of the order of 100 MPa. Hence, as a first assessment, the electrical resistance measurements of the CNT fiber could be used in such materials to point out whether a malfunction or an overload during service has been occurred. This of course will produce damage, and will definitely shift the mechanical stress – $\Delta R/R_0$ measurements.

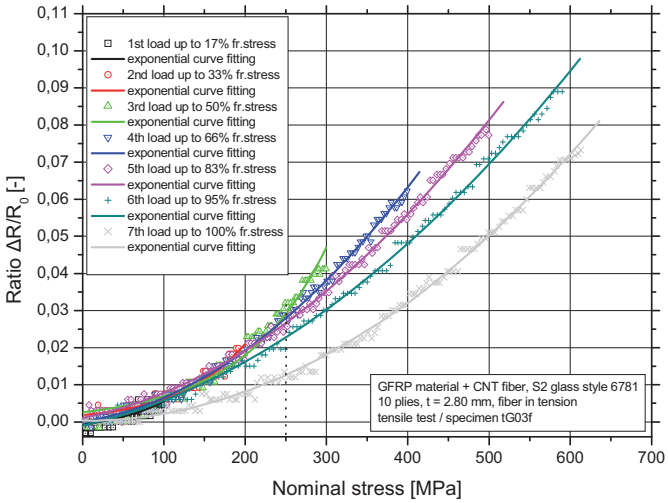

Fig. 4. Correlation between coupon's mechanical stress and PVA-CNT fiber's electrical resistance measurements.

3.2 Integral composite structure part test results

Appropriate fixtures had been manufactured to monotonic test the integral structure in three point bending. Figure 5 shows typical photographs of the structure during various loading steps of the monotonic mechanical loading till fracture.

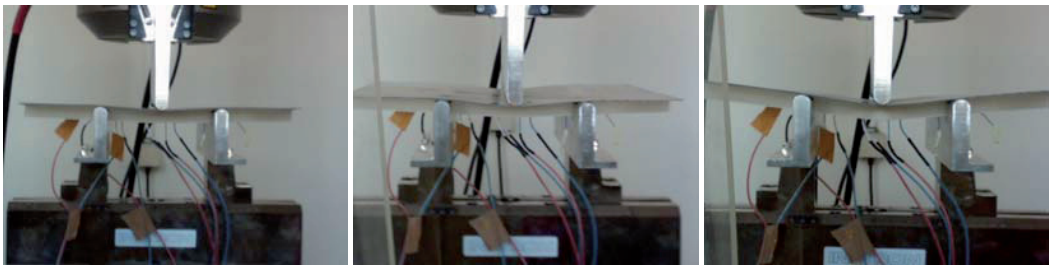

(a) (b) (c)

Fig. 5. Testing photographs of the integral structure with embedded CNT fibers (a) low loading up to 30% (b) medium loading up to 60% and (c) loading up to 95% of the fracture load, respectively.

The electrical resistance measurements were calculated as $\Delta R/R_0$ values for the four PVA-CNT fibers. The results of the values $\Delta R/R_0$ had been converted to axial strain by the numerous tensile and three point bending tests in coupons; strain results with the increasing applied load for all PVA-CNT fibers can be seen in Figure 6. The values of the electrical resistance change are almost linear with the increasing applied load of the structure. Worth noting is the high values of the PVA-CNT fiber No2 after 3.8 kN; the readings follows different increasing slope with continuously increasing applied load. This is evidence of damage occurring at the PVA-CNT fiber's local region; hence, it is eminent that fracture of the structure will take place nearby. As expected, fracture took place in the stiffener close to the PVA-CNT fiber No2. Figure 7 shows the photograph of the fractured stiffener and the location of the respective PVA-CNT fiber.

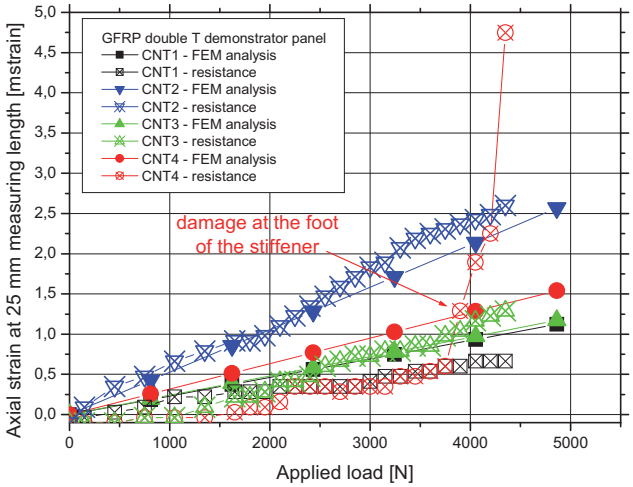

Fig. 6. Calculated strain values of the embedded PVA-CNT fibers versus experimental values of the integral GFRP structure.

Fig.7. Photograph of the fractured stiffener of the integral GFRP structure and PVA-CNT fibers; PVA-CNT fiber No2 recorded essential damage before fracture.

4 Finite Element Analysis

4.1 Modelling of the structure

A finite element model of the specimen was developed using the ANSYS finite element software package. The specimen was modeled with 4 node laminated shell elements. A relatively fine mesh was used in order to avoid locking problems, Figure 8. There were three areas with different properties: (a) The skin with 4 plies, (b) the skin-stringer foot with 8 plies and (c) the stringer blades with 8 plies, Figure 8. The stacking sequence of each area is listed in Table 1.

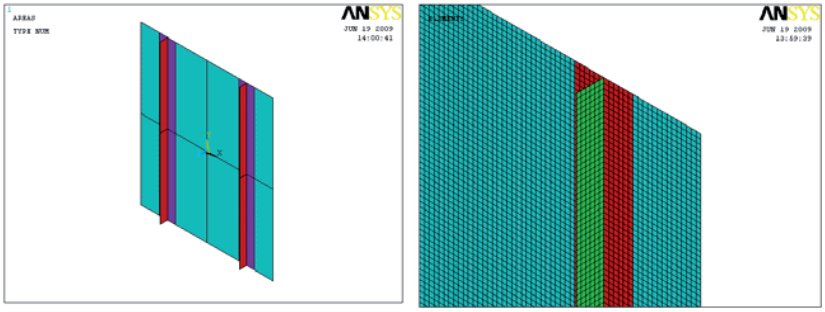

Fig. 8. Meshing of the integral structure and meshing detail of the structure at the location of the stiffener.

Each ply of glass is a biaxial fabric (0.25 mm cured ply thickness) with almost the same properties along the weft and warp direction. For this purpose, the glass fabric was modelled as a 2D orthotropic material. The assumed material properties were E_{11} = 22 GPa, E_{22} = 22 GPa, ν_{12} = 0.17 and G_{12} = 3.5 GPa.

The metallic supports were symmetrically positioned about the main center line, at a distance of 130 mm from each other. In the FE model, a prescribed displacement of 6 mm was applied along the main center line. The selected solution sequence was non linear static analysis for large displacements (SOL 106) with the load being divided into 20 sub-steps.

Table 1. Stacking sequence of specimen areas (0˚ is collinear with the specimen's longitudinal axis).

Area	Stacking Sequence
Skin	0˚ / 45˚ / 45˚ / 0˚
Skin stringer foot	0˚ / 45˚ / 45˚ / 0˚ / 45˚ / 0˚ / 0˚ / 45˚
Stringer blade	45˚ / 0˚ / 0˚ / 45˚ / 45˚ / 0˚ / 0˚ / 45˚

4.2 Results and discussion

Figure 9 shows the Von Mises equivalent stress distribution of the structure for 1 mm vertical displacement of the middle span of the structure. As expected, maximum stresses are deployed at the top of the stiffener; a maximum stress of approximate 100 MPa is noticed. Given from the axial coupon tests that the maximum fracture stress was of the order of 600 MPa, the maximum calculated stress for 6 mm vertical displacement will be of the same magnitude. Hence, the calculated results

can be judged as very good results. Figure 9 shows the strain distribution of the structure for the same vertical displacement of the middle span of the structure.

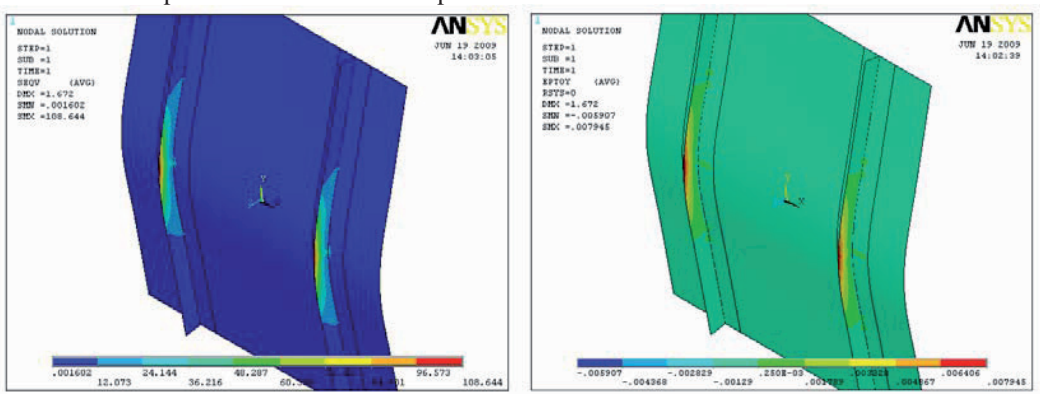

Fig.9. Von Mises equivalent stress and strain distribution of the integral structure for 1 mm vertical displacement, respectively.

FEM calculated strain versus applied load is plotted for the four CNT locations. This is a meaningful result because it is offered for comparison with the experimentally measured strain from the resistance change values of the CNT fibers. At this point is must be noted that, the actual CNT fibers are 25 mm long, so in reality such a sensor measure the average strain along this length. For comparison reasons, the longitudinal strains shown in Figure 6 are averaged at each location over a line of nodes that extend to a length of 25 mm more or less.

Current FEM used linear analysis and hence, strain increases linear with the increasing applied load. A great prediction of the strain measurements is noticed for the case of the CNT fibers No 2 and 3. Analysis showed fair results for the other two CNT fibers. Nevertheless, it can clearly be seen that the embedded CNT fibers can be used for sensing purposes in non-conductive composite structures.

References

1. K. Schulte, Ch. Baron, Compos. Sci. Technol., **36**, 349 (1989)
2. AS Kaddour, FAR Al-Salehi, STS Al-Hassani, MJ Hinton, Compos. Sci. Technol., **51**, 377 (1994)
3. P.E. Irving, C. Thiagarajan, Smart Mater. Struct., **7**, 456 (1998)
4. D.C. Seo, J.J. Lee, Comp. Struct., **47**, 525 (1999)
5. J.C. Arby, S. Bochard, A. Chateauminois, M. Salvia, G. Giraud, Compos. Sci. Technol., **59**, 925 (1999)
6. N. Muto, Y. Arai, S.G. Shin, H. Matsubara, H. Yanagida, M. Sugita, T. Nakatsuji, Compos. Sci. Technol., **61**, 875 (2001)
7. B. Vigolo, A. Penicaud, C. Coulon, C. Sauder, R. Pailler, C. Journet, P. Bernier, P. Poulin, Science, **290**, 1331 (2000)
8. P. Poulin, B. Vigolo, P. Launois, Carbon, **40**, 1741 (2002)
9. P. Miaudet, S. Badaire, A. Derré, M. Maugey, V. Pichot, P. Launois, P. Poulin, C. Zakri, Nanoletters, **5**, 2212 (2005)
10. N.D. Alexopoulos, C. Bartholome, P. Poulin, Z. Marioli-Riga, Compos. Sci. Technol., **70**, 260 (2010)